LA-UR- 99-282

ANISOTROPIC MULTI-RESOLUTION ANALYSIS IN 2D, APPLICATION TO LONG-RANGE CORRELATIONS IN CLOUD MM-RADAR FIELDS

CONF-990407--

Anthony B. Davis

Los Alamos National Laboratory,
Space & Remote Sensing Science Group (NIS-2)
P.O. Box 1663 (Mail Stop C-323),
Los Alamos, NM 87545, USA.

&

Eugene Clothiaux

The Pennsylvania State University,
Department of Meteorology
502 Walker Building,
University Park, PA 16802, USA.

ABSTRACT

Because of Earth's gravitational field, its atmosphere is strongly anisotropic with respect to the vertical; the effect of the Earth's rotation on synoptic wind patterns also causes a more subtle form of anisotropy in the horizontal plane. We survey various approaches to statistically robust anisotropy from a wavelet perspective and present a new one adapted to strongly non-isotropic fields that are sampled on a rectangular grid with a large aspect ratio. This novel technique uses an anisotropic version of Multi-Resolution Analysis (MRA) in image analysis: we form a tensor product of the standard dyadic Haar basis, where the dividing ratio is $\lambda_z = 2$, and a nonstandard triadic counterpart, where the dividing ratio is $\lambda_x = 3$. The natural support of the field is therefore 2^n pixels (vertically) by 3^n pixels (horizontally) where n is the number of levels in the MRA. The natural triadic basis includes the French top-hat wavelet which resonates with "bumps" in the field whereas the Haar wavelet responds to "ramps" or "steps". The complete 2D basis has one scaling function and five wavelets.

The resulting anisotropic MRA is designed for application to the liquid water content (LWC) field in boundary-layer clouds, as the prevailing wind advects them by a vertically pointing mm-radar system. Spatial correlations are notoriously long-range in cloud structure and we use the wavelet coefficients from the new MRA to characterize these correlations in a multifractal analysis scheme. In the present study, the MRA is used (in synthesis mode) to generate fields that mimic cloud structure quite realistically although only a few parameters are used to control the randomness of the LWC's wavelet coefficients.

1. INTRODUCTION

Multifractal analysis has proven invaluable in a wide variety of applications ranging from chaos theory and turbulence (where it was first conceived) to high-energy particle physics and cosmology. Power-law statistics also arise in many laboratory-scale (e.g., materials science) experiments as well as in the field (e.g., in geophysics). Wavelet theory is well-suited to capture phenomena that occur on a broad range of scales, with arbitrary intensity and degree of localization. Wavelet-tools have thus enhanced our understanding of nonlinear dynamical systems, some of which have so many degrees of freedom that their behavior may just as well be considered random. So wavelet transforms (WTs) and multifractal formalism have had a natural and prosperous marriage [1].

DISCLAIMER

Curiously, wavelet-multifractal analyses of data have been almost exclusively based on the Continuous WT (CWT). In this work, we try to repair this unjustified neglect of the simpler Discrete WT (DWT). We also try to break through the "barrier of isotropy" in 2D settings.

In the next section, we survey wavelet- assisted multifractal data analysis in 1D and illustrate the lesser-known methods with data pertaining to cloud structure. In section 3, we recast in discrete wavelet space procedures for generating selected scale-invariant stochastic models; some are well-known but monofractal (fractional Brownian motion), others are less-known and strongly multifractal (bounded multiplicative cascades). Section 4 is devoted to 2D issues: How should we treat data that is statistically isotropic? and What are our options in highly anisotropic situations? Again, our motivation for relaxing the all-too-standard assumption of isotropy is rooted in atmospheric processes: cloud formation and maintenance in presence of strong stratification.

2. WAVELETS & MULTIFRACTAL DATA ANALYSIS IN 1D

2.1. Useful Wavelet Definitions

We assume in the following that data

$$f(x),\ 0 \le x < L_f, \tag{1}$$

is given on a regular grid of constant $\ell = 1$; there can be several f's in an ensemble of interest, not necessarily of equal lengths.

2.1.1. *Continuous Wavelet Transform:*

Assuming $\psi(x)$ is a real admissible (zero-mean, at least once-oscillating) wavelet, we define the CWT of $f(\cdot)$ as

$$T_\psi[f](a,b) = \frac{1}{a}\int f(x)\psi\left(\frac{x-b}{a}\right)\,dx, \tag{2a}$$

where

$$\begin{cases} 0 < a < L = \min_f\{L_f\} \\ 0 \le b < L \end{cases}, \tag{2b}$$

assuming periodic extension in both directions. In practical computations, the pair (a,b) has integer values (in pixel units). Notice that we use an L_1 (rather than the more standard L_2) normalization in (2a).

We can define a similar integral transform $T_\varphi[f](a,b)$ for the scaling function $\varphi(x)$, which is essentially a non-oscillating "wavelet."

Gaussian-based examples:

$$\varphi_G(x) = \exp[-x^2/2]/\sqrt{2\pi}\ ; \tag{3a}$$

$$\psi_{\partial G}(x) = -\partial_x\varphi_G(x) = x\varphi_G(x); \tag{3b}$$

$$\psi_{Mh}(x) = \partial_x{}^2\varphi_G(x) = (x^2-1)\varphi_G(x). \tag{3c}$$

The latter is the "Mexican hat" wavelet.

2.1.2. *Discrete Wavelet Transform:*

We will work in the frame of dyadic (λ=2) or triadic (λ=3) Multi-Resolution Analysis or "MRA", *à la* Mallat [2], where

$$n_\lambda(L_f) = \mathrm{int}(\log_\lambda L_f), \tag{4}$$

is a key quantity: the number of octaves (λ=2) or powers of 3 in the data. Here we narrow our focus onto the following subset of (a,b)'s:

$$\begin{cases} a_j(\lambda) = \lambda^j,\ j = 0,\ldots,j_{\max} \\ b_{ji}(\lambda) = i\lambda^j,\ i = 0,\ldots,\lambda^{(j_{\max}-j)}-1 \end{cases} \tag{5}$$

where $j_{\max} = n_\lambda(L)-1$. The total number of points in this subset is

$$\text{card}[\{a_j,b_{ji}\}] = (\lambda^{n_\lambda(L)}-1)/(\lambda-1). \tag{6}$$

The break-down of this MRA is:

wavelet coefficients in MRA: $(\lambda-1)\times\text{card}[\{a_j,b_{ji}\}]$;
scaling-function coeficient required at $j_{\max}$: 1;
total number of coefficients in MRA: $\lambda^{n_\lambda(L)}$.

In the following, we use $1_S(x)$ to designate the indicator function of interval S: $1_S(x) = 1$, if $x \in S$; $1_S(x) = 0$, otherwise.

$\lambda = 2$: The famous Haar basis is spawned by

$$\begin{cases} \varphi_H(x) = 1_{[0,2)}(x)/2 \\ \psi_H(x) = -1_{[0,1)}(x)+1_{[1,2)}(x) \end{cases} \tag{7}$$

with the required (lack of L_2) normalization. Notice how, apart from a unitary translation, the Haar scaling-function and wavelet in (7) are piece-wise constant approximations of the Gaussian (3a) and its anti-derivative (3b).

The computational MRA "trick," leading to algorithms with $O(N)$ complexity [2], is based on the remark that $\psi_H(x)$ in Eq. (7) can be rewritten as $2[-\varphi_H(x/2)+\varphi_H((x-1)/2)]$.

$\lambda = 3$:

$$\begin{cases} \varphi_3(x) = 1_{[0,3)}(x)/3 \\ \psi_a(x) = -1_{[0,1)}(x) \qquad +1_{[2,3)}(x) \\ \psi_s(x) = +1_{[0,1)}(x)-2\times 1_{[1,2)}(x)+1_{[2,3)}(x) \end{cases} \tag{8}$$

In this natural extension of the generators of the Haar basis in (7), $\psi_s(x)$ —sometimes called the "(French) top-hat" wavelet— is a piece-wise constant approximation to $\psi_{Mh}(x)$ in (3c).

2.2. Multifractal Analysis

2.2.1. *Structure Functions:*

Structure functions [3] are 2-point statistics for a given "lag" r defined any "order" q:

$$\langle |f(x+r)-f(x)|^q \rangle_{x,f} \sim r^{\zeta(q)} \tag{9}$$

where the subscript "x,f" denotes the spatial (or x-) averaging and an optional ensemble (or f-) averaging. In Eq. (9) we have spelled out the power-law representation of structure functions that we expect in scale-invariant (or "fractal") signals. In practical applications ("physical" fractals), the power-law behavior in (9) applies over a finite scaling range $[r_{\min},r_{\max}]$.

With wavelets, structure functions in (9) are generalized to:

$$\langle |T_\psi[f](a,b)|^q \rangle_{b,f} \sim a^{\zeta(q)} \tag{10}$$

for $[a_{\min},a_{\max}]$. In fact, (9) is a special case of (10) for the following choice of wavelet [4]:

$$\psi_{\text{poor\_man}}(x) = \delta(x-1) - \delta(x), \tag{11}$$

with $a = r$. Muzy *et al.* [4] describe conditions on f's singularity spectrum and/or ψ's number of oscillations under which the same $\zeta(q)$'s are obtained using (9) and (10), generally with a different

set of prefactors however. For $q \geq 0$, single-oscillation wavelets are sensitive to all orders of (Hölder) singularity less than unity, i.e., everywhere $f(x)$ is non-differentiable. In the remainder, we assume this to be true.

Having established an identity between $\zeta(q)$ exponents using different wavelets, including the degenerate case in (11), it is important to be able to compare the scaling regimes. However, different wavelets have different connections between the scale-parameter a and the lag r. For instance, we should use

$$r_j(\lambda) = (\lambda-1)a_j(\lambda), j = 0,\ldots j_{\max} \tag{12a}$$

for $\psi_H(x)$ and $\psi_a(x)$, respectively, in DWTs with $\lambda = 2,3$. There is no general rule for CWTs. One can use the distance between the extrema which yields 2 for $a = 1$ when using $\psi_{\partial G}(x)$. Alternatively, one can use

$$r_1 = 2 \times \int_0^\infty x\,\psi(x)dx \,/\, \int_0^\infty \psi(x)dx \tag{12b}$$

for a properly centered ($\int x\psi(x)dx = 0$) wavelet; for $\psi_{\partial G}(x)$, this again yields $r_1 = 2$ for $a = 1$.

2.2.2. *Partition Functions:*

In lieu of the wavelet-based generalization of structure functions in (10), one can use

$$Z(q,a) = \left\langle \sum_{b\in S_a} |T_\psi[f](a,b)|^q \right\rangle_f \tag{13}$$

the "partition function," where S_a is a subset of all b's for a given a. For partition functions, the scaling in Eqs. (9–10) becomes

$$Z(q,a) \sim a^{\tau(q)}. \tag{14}$$

The statistical quantities in (10) and (13–14) are of course related:

$$\langle |T_\psi[f](a,b)|^q \rangle_{b,f} = Z(q,a) \,/\, \mathrm{card}[S_a], \tag{15}$$

noting that the denominator depends only on ψ and a. In some situations, it should be taken as the mean of a narrowly-distributed random variable that is quasi-independent of f (hence the above factoring). The relation between $\tau(q)$ and $\zeta(q)$ depends on the spatial (b-wise) sampling strategy.

"Continuous" spatial sampling:

Consider first a CWT approach based on

$$S_a = \{b \in [0,L);\, 0 \leq b < L\}, \tag{16}$$

recalling that a and b are actually integers; so $\mathrm{card}[S_a] = L$ in Eq. (15) and $\tau_c(q) = \zeta(q)$.

This approach is amenable to computational enhancement by using a "non-decimated" DWT (nd-DWT) [5] at a small cost in the sampling: $\mathrm{card}[S_a] = L-(\lambda-1)\sum_{j'=0}^{j(a)} \lambda^{j'} = L+1-\lambda^{j(a)+1}$.

"WTMM" spatial sampling:

Following Muzy *et al.* [4], consider the (Continuous) Wavelet Transform Maximum Modulus or "WTMM" approach based on

$$S_a = \{b;\, |T_\psi[f](a,b)| \text{ is locally max}\}. \tag{17}$$

Here, $\mathrm{card}[S_a] \approx L/a$ because, at least for scale-invariant data, extrema in $T_\psi[f](a,b)$ with respect to b necessarily alternate at scales $\approx a$ which is the characteristic smoothing scale of the kernel in (2a). So we find $\tau(q) = \zeta(q)-1$.

WTMM methodology is much more than a sampling strategy and the interested reader is referred to recent review papers [6]. WTMM approaches indeed clarify the deep connections between wavelet theory and multifractal formalism, including thermodynamic analogies.

"DWT" spatial sampling:

Consider now a DWT-based approach with

$$S_a = S_j = \{b \in [0,L);\ b = b_{ji}(\lambda)\}. \tag{18}$$

Since card[S_a] = $\lambda(j_{max}-j) \approx L/a$, as for WWTM sampling, we again find $\tau(q) = \zeta(q)-1$.

By using the "box-car" function $1_{[0,1)} = 2\times\varphi_H(x/2)$ instead of the wavelet in (2a), we retrieve the (dyadic) "box-counting" method. In turn, this leads to the original [7] definition of $\tau(q)$ for a (non-negative) measure $\mu(x)$:

$$\sum_{b\in S_a}[\int_b^{b+a}\mu(x)dx\,]^q = \sum_{b\in S_a}|aT_{\varphi_H}[\mu](a,b)|^q \sim a^{\tau(q)} \tag{19}$$

2.3. Illustration with Cloud Data

Figure 1 shows two traces of cloud liquid water content (mass of droplets per unit of volume) measured by aircraft penetrations into a marine stratocumulus deck. The variability and its spatial inhomogeneity —the variability of the variability— are remarkable but not untypical in geophysics; see [8a] for details.

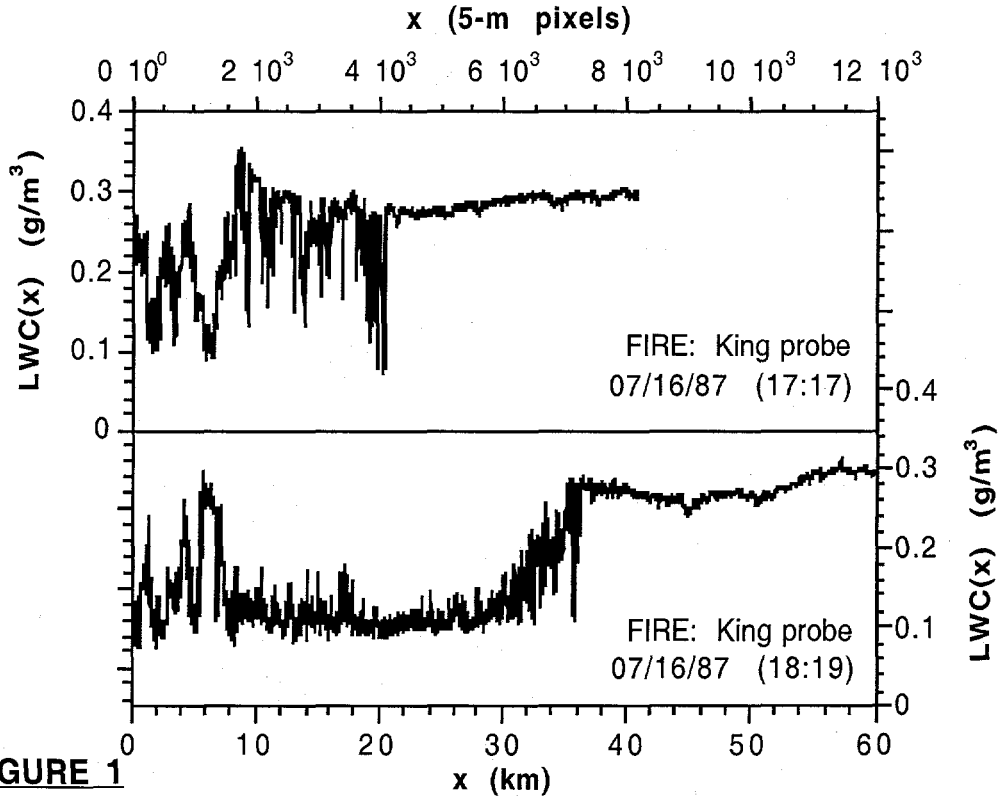

FIGURE 1

Figure 2 shows the similar scaling at $q = 2$ obtained for structure functions [8b] —and selected wavelet counterparts— using various sampling procedures on the data in Fig. 1.

For obvious reasons, DWT sampling (×'s and +'s in Fig. 2) yields noisier estimates but it has the advantage of MRA's computational efficiency. This makes it an attractive approach for "on-

line" multifractal analysis of data as fast as it is collected. A systematic comparison of wavelet-multifractal data analyses is in preparation and will be published elsewhere.

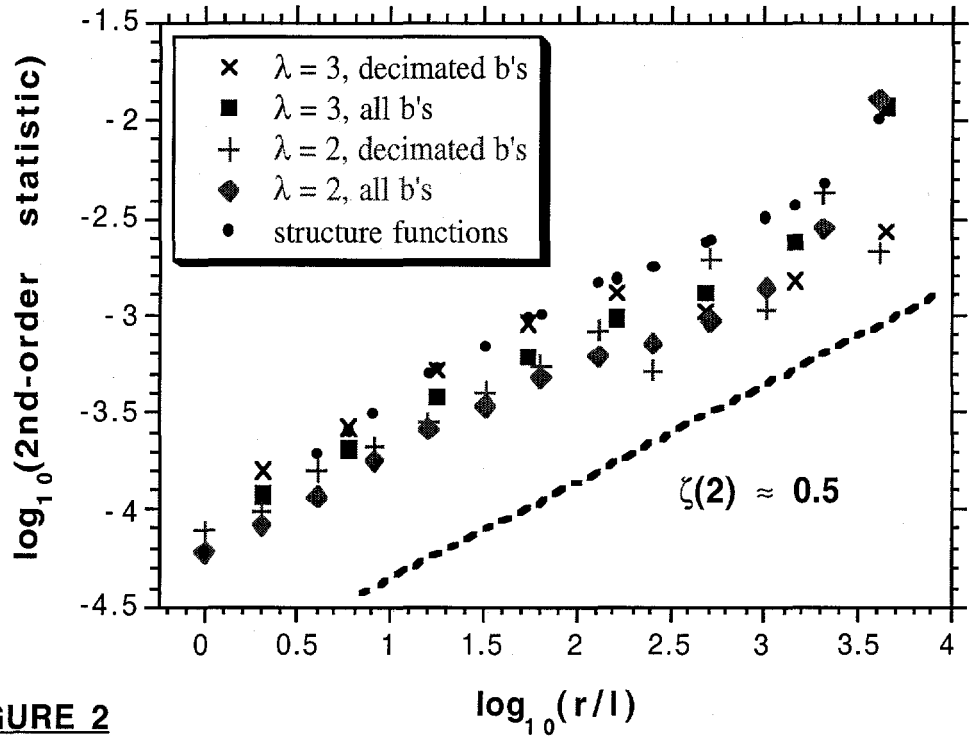

FIGURE 2

3. CASCADE MODELING WITH THE INVERSE DWT (IDWT) IN 1D

In this section we briefly describe methods to generate mono- and multi-fractal data with known properties in discrete wavelet space [9]. The length of each realization is set by

$$L = \lambda j_{\max}+1 \tag{20}$$

where $\lambda = 2$ or 3. Thus, $n_\lambda(L) = j_{\max}+1 >> 1$.

3.1. Dyadic Cascades ($\lambda = 2$)

3.1.1. *fractional Brownian motion (fBm):*

It has been shown [10] that a close analog of fBm is obtained by randomly activating DWT coefficients according to

$$T_{\psi_H}[fBm](a_j,b_{ji}) = N(0,1)(2a_j)^{H_2} \tag{20a}$$

where H_2 is the only free parameter and the $N(0,1)$'s are independent pseudo-Gaussian deviates with zero-mean and unit-variance. This leads to $\zeta(q) = qH_2$ in Eq. (10). The L–1 wavelet coefficients in (20a) are completed by

$$T_{\varphi_H}[fBm](a_{j_{\max}},0) = 0 \tag{20b}$$

in the MRA decomposition required for the IDWT synthesis of $f(x)$.

3.1.2. *bounded (p,H-model) cascades:*

As counterpoint to fBm's characteristic monoscaling ($\zeta(q)/q = constant$), we can recast deterministically the construction of "bounded" multiplicative cascade models [11,17] in a DWT context:

$$T_{\psi_H}[\ln f](a_j,b_{ji}) = \pm\ln\left(\frac{1+(2p-1)(2a_j/L)^H}{1-(2p-1)(2a_j/L)^H}\right) \tag{21a}$$

where the sign is random, and

$$T_{\varphi_H}[\ln f](a_{j_{max}},0) = \frac{1}{2}\sum_j \ln(1-(2p-1)^2(2a_j/L)^{2H}) \tag{21b}$$

Finally, we exponentiate the IDWT's outcome.

In the log's, we recognize respectively the ratio and harmonic mean of the two multi-plicative weights. In this micro-canonical [12] model the weights are purposefully designed to exactly conserve the total measure (at each cascade step and in each realization). For $H = 0$, we retrieve the one-parameter "p-model" that Meneveau and Sreenivasan [13] proposed for the dissipation field in turbulence. Marshak *et al.* [11] showed that, for $H > 0$, this model has $\zeta(q) = \min\{qH,1\}$ independent of p.

3.2. Triadic Cascades ($\lambda = 3$)

3.2.1. *fractional Brownian motion:*

Generalization of the above DWT-based model for fBm-type processes to this case is straightforward; we will just state the recipe:

$$T_{\psi_a}[fBm](a_j,b_{ji}) = N(0,1)(2a_j)^{H_2}; \tag{22a}$$

$$T_{\psi_s}[fBm](a_j,b_{ji}) = N(0,1)(6a_j)^{H_2}; \tag{22b}$$

$$T_{\varphi_3}[fBm](a_{j_{max}},0) = 0. \tag{22c}$$

3.2.2. *bounded cascades:*

Micro-canonical conservation allows for 2 parameters in this case; the 3 weights are:

$$W_1(j,i) = 1+(3p_1-1)(3a_j/L)^H; \tag{23a}$$

$$W_2(j,i) = 1+(3p_2-1)(3a_j/L)^H; \tag{23b}$$

$$W_3(j,i) = 3-W_1(j,i)-W_2(j,i). \tag{23c}$$

Now let

$$\{k_1,k_2,k_3\} = \text{perm}\{1,2,3\} \tag{24}$$

denote a random permutation of the indices. DWT coefficients are then computed as:

$$T_{\psi_a}[\ln f](a_j,b_{ji}) = \ln[W_{k_3}(j,i)/W_{k_1}(j,i)]; \tag{25a}$$

$$T_{\psi_s}[\ln f](a_j,b_{ji}) = \ln[W_{k_3}(j,i)W_{k_1}(j,i)/W_{k_2}(j,i)^2]; \tag{25b}$$

$$T_{\varphi_3}[\ln f](a_{j_{max}},0) = \frac{1}{3}\sum_j \ln[W_1(j,i)W_2(j,i)W_3(j,i)]. \tag{25c}$$

4. WAVELET-MULTIFRACTAL ANALYSIS AND MODELING IN 2D

4.1. Definitions (Isotropic Case)

We now assume the data

$$f(\boldsymbol{x}) = f(x_1,x_2),\ 0 \le x_1 < L_1,\ 0 \le x_2 < L_2 \tag{26}$$

is given on a regular 2D grid with $\ell_1 = \ell_2 = 1$. 2D generalizations of the Gaussian wavelets in Eqs. (3a–c) lead either to scalar or vector formulations. In the following, we will use

$$\varphi_G(\boldsymbol{x}) = \frac{1}{2\pi}\exp[\frac{-\boldsymbol{x}^2}{2}] = \frac{1}{2\pi}\exp[\frac{-(x_1^2+x_2^2)}{2}]. \tag{27}$$

4.1.1. *CWTs with scalar wavelets:*

The popular 2D Mexican-hat CWT is:

$$T_{\psi_{Mh}}[f](a,\boldsymbol{b}) = \frac{1}{a^2}\int f(\boldsymbol{x})\psi_{Mh}\left(\frac{\boldsymbol{x}-\boldsymbol{b}}{a}\right) d^2\boldsymbol{x} \tag{28a}$$

where $\psi_{Mh}(\boldsymbol{x}) = \nabla^2\varphi_G(\boldsymbol{x}) = (x_1^2+x_2^2-2)\varphi_G(x_1,x_2)$.

4.1.2. *CWTs with vector wavelets:*

The Gaussian's 1st-order partial derivatives can also be used in the pair of transforms [14]:

$$T_{\psi_m}[f](a,\boldsymbol{b}) = \frac{1}{a^2}\int f(\boldsymbol{x})\psi_m\left(\frac{\boldsymbol{x}-\boldsymbol{b}}{a}\right) d^2\boldsymbol{x} \tag{28b}$$

for m=1,2 where $\psi(\boldsymbol{x}) = \{\psi_1(\boldsymbol{x}),\psi_2(\boldsymbol{x})\}^T = -\left\{\frac{\partial}{\partial x_1}, \frac{\partial}{\partial x_2}\right\}^T\varphi_G(\boldsymbol{x})$, letting superscript "T" mean transpose. These filters are commonly used in edge-detection applications.

Whether the CWT's outcome is scalar or vector, the wavelet domain is:

$$\begin{cases} 0 < a < L = \min_m\{L_m, m = 1,2\} \\ 0 \le b_m < L\ (m = 1,2) \end{cases}, \tag{28c}$$

assuming periodic extensions.

4.1.3. *DWTs with* $\lambda = 2,3$:

In isotropically discretized wavelet space, the scale parameter a_j is as in Eq. (5), but position naturally become a vector:

$$\boldsymbol{b}_{j,\boldsymbol{i}}(\lambda) = \boldsymbol{i}\lambda^j,\ i_m = 0,\ldots,\lambda^{j_{max}-j}-1\ (m = 1,2),$$

and the total number of points is

$$\text{card}[\{a_j,\boldsymbol{b}_{j,i}\}] = (\lambda^{2n_\lambda(L)}-1)/(\lambda^2-1). \tag{29}$$

The break-down of a 2D MRA using tensor products of the basis-generators in (7–8) is:

2D MRA wavelet coef's: $(\lambda^2-1)\times\text{card}[\{a_j,\boldsymbol{b}_{ji}\}]$;
scaling-function coeficient required at j_{max}: 1;
total number of coefficients in 2D MRA: $(\lambda^2)^{n_\lambda(L)}$.

Because the scaling functions and wavelets in 1D MRA can be likened to the 0th-, 1st- and 2nd-order derivatives of the Gaussian, their λ^2 different tensor products are akin to the various partial derivatives of the 2D Gaussian. E.g., $\varphi_H(x_1)\psi_H(x_2)$ or $\varphi_3(x_1)\psi_a(x_2)$ will approximate $\psi_2(\boldsymbol{x})$ and $\psi_s(x_1)\psi_s(x_2)$ resembles $\psi_{Mh}(\boldsymbol{x})$.

4.2. Isotropic Partition Functions

There is no fundamental difference between 1D and 2D multifractal analyses, standard or wavelet-based, as long as it is kept isotropic (no preferred directions at any scale). Partition functions still scale as $Z(q,a) \sim a^{\tau(q)}$; only the precise way they are computed changes.
Scalar-wavelet approach using Eq. (28a):

$$Z(q,a) = \left\langle \sum_{\boldsymbol{b}\in S_a} |T_\psi[f](a,\boldsymbol{b})|^q \right\rangle_f \tag{30a}$$

Vector-wavelet approach using Eq. (28b):

$$Z(q,a) = \left\langle \sum_{\boldsymbol{b}\in S_a} \|\boldsymbol{T}_\psi[f](a,\boldsymbol{b})\|^q \right\rangle_f \tag{30b}$$

where

$$\|\boldsymbol{T}_\psi[f](a,\boldsymbol{b})\| = \sqrt{T_{\psi_1}[f](a,\boldsymbol{b})^2 + T_{\psi_2}[f](a,\boldsymbol{b})^2}\,. \tag{31}$$

2D structure functions can be defined, with and without isotropy, as $\langle |f(\boldsymbol{x}+\boldsymbol{r})-f(\boldsymbol{x})|^q \rangle_{\boldsymbol{x},f}$ but they have rarely been used in data analysis, except for $q = 2$ [15]. The closest wavelet analog is $\langle \|\boldsymbol{T}_\psi[f](a,\boldsymbol{b})\|^q \rangle_{\boldsymbol{b},f} = Z(q,a)/\mathrm{card}[S_a]$ from (30b) and it scales as $a^{\zeta(q)}$.

As in 1D, there are several sampling strategies: Continuous, WTMM, and DWT.

"Continuous" spatial sampling:

$$S_a = \{\boldsymbol{b};\ 0 \le b_1, b_2 < L\} \tag{32}$$

We again must account for the dimensionality effect on the scaling: $\tau_c(q) = \zeta(q) = \tau(q)+2$, since $\mathrm{card}[S_a] = L^2$ for all a's.

Because 2D datasets tend to be quite large, this is a situation where the computational acceleration of nd-DWTs is welcome.

"WTMM" spatial sampling:

$$S_a = \{\boldsymbol{b};\ \|\boldsymbol{T}_\psi[f](a,\boldsymbol{b})\| \text{ is locally max}\} \tag{33}$$

with $\mathrm{card}[S_a] \approx (L/a)^2$ because of correlations extending over a range $\approx a$ in wavelet space.

Arrault *et al.* [16] successfully applied 2D-WTMM methodology to synthetic surfaces, both Gaussian and multifractal, with specified roughness, as well as to some high-resolution satellite images of turbulent cloud structures.

"DWT " spatial sampling:

$$S_a = S_j = \{\boldsymbol{b};\ \boldsymbol{b} = \boldsymbol{b}_{j,i}(\lambda)\} \tag{34}$$

with $\mathrm{card}[S_a] = \lambda^{2(j_{max}-j)} \approx (L/a)^2$.

Here again the disadvantage of increased statistical noise is off-set by the possibility of $O(N)$ efficiency in applications where it is desirable to obtain multifractal statistics almost as fast as the images are captured.

4.3. Approaches to Anisotropy

We list here a few ways of describing anisotropy in 2D data.

4.3.1. *Using Scalar Wavelets:*

Here the scale parameter becomes a vector

$$\boldsymbol{a} = (a_1, a_2)^T \tag{35}$$

in the generalized form of Eq. (28a):

$$T_\psi[f](\boldsymbol{a},\boldsymbol{b}) = \frac{1}{a_1 a_2}\int f(\boldsymbol{x})\psi\left(\frac{x_1-b_1}{a_1},\frac{x_2-b_2}{a_2}\right)\,\mathrm{d}^2\boldsymbol{x}. \tag{36}$$

The wavelet itself can be axi-symmetric, as in $\psi_{\mathrm{Mh}}(\boldsymbol{x})$. Or else it can have less symmetry, as in $(\partial/\partial x_1)(\partial/\partial x_2)\varphi_{\mathrm{G}}(\boldsymbol{x})$ which is a "checker-board" filter of sorts, or $\psi_1(\boldsymbol{x}) = -(\partial/\partial x_1)\varphi_{\mathrm{G}}(\boldsymbol{x})$ which is a standard edge-detector.

4.3.2. *Using Vector Wavelets:*

Here we can simply use the directional information in the wavelet transform pair (28b):

$$\begin{cases} \cos\alpha(a,\boldsymbol{b}) = T_{\psi_1}[f](a,\boldsymbol{b}) / \|\boldsymbol{T}_\psi[f](a,\boldsymbol{b})\| \\ \sin\alpha(a,\boldsymbol{b}) = T_{\psi_2}[f](a,\boldsymbol{b}) / \|\boldsymbol{T}_\psi[f](a,\boldsymbol{b})\| \end{cases} \tag{37}$$

A quantitative test of anisotropy is to examine the possibly scale-dependent distribution of α for the existence of modes.

4.3.3. *Custom Multi-Resolution Analysis:*

A simple and potentially useful way of measuring and simulating anisotropy is to use (I)DWTs based on tensor products of dyadic and triadic scaling functions and wavelets defined in Eqs. (7–8).

Given some 2D data (maybe on an oblong support), we first decide which axis is assigned to the dyadic branching and which to the triadic, e.g., $\lambda_1 = 3$, $\lambda_2 = 2$. We then compute

$$n_m(\lambda_m) = \mathrm{int}[\log_{\lambda_m} L_m] \;(m = 1,2) \tag{38}$$

and reckon the number of cascade steps:

$$n_{\mathrm{c}}(\boldsymbol{L}) = n_{\mathrm{c}}(L_1,L_2) = \min\{n_1(\lambda_1),n_2(\lambda_2)\}. \tag{39}$$

The constants used in the anisotroptic (I)DWT —via 2D MRA— are given in Fig. 3a. Figure 3b is a schematic of this MRA where the total number of points is

$$\mathrm{card}[\{\boldsymbol{a}_j,\boldsymbol{b}_{j,i}\}] = [(\lambda_1\lambda_2)^{n_{\mathrm{c}}(\boldsymbol{L})}-1]/[\lambda_1\lambda_2-1]. \tag{40}$$

The break-down of the custom 2D MRA is:

2D MRA wavelet coef's: $(\lambda_1\lambda_2-1)\times\mathrm{card}[\{\boldsymbol{a}_j,\boldsymbol{b}_{ji}\}]$;
scaling-function coefficient required at $j_{\max}$: 1;
total number of coef's in 2D MRA: $(\lambda_1\lambda_2)^{n_{\mathrm{c}}(\boldsymbol{L})}$.

$\varphi(x,y) = 1/6$ $\psi_1(x,y) = +1/3$ $\psi_2(x,y) = -1/2$ $\psi_3(x,y) = -1$ $\psi_4(x,y) = +1/2$ $\psi_5(x,y) = +1$	$\varphi(x,y) = 1/6$ $\psi_1(x,y) = +1/3$ $\psi_2(x,y) = 0$ $\psi_3(x,y) = 0$ $\psi_4(x,y) = -1$ $\psi_5(x,y) = -2$	$\varphi(x,y) = 1/6$ $\psi_1(x,y) = +1/3$ $\psi_2(x,y) = +1/2$ $\psi_3(x,y) = +1$ $\psi_4(x,y) = +1/2$ $\psi_5(x,y) = +1$
$\varphi(x,y) = 1/6$ $\psi_1(x,y) = -1/3$ $\psi_2(x,y) = -1/2$ $\psi_3(x,y) = +1$ $\psi_4(x,y) = +1/2$ $\psi_5(x,y) = -1$	$\varphi(x,y) = 1/6$ $\psi_1(x,y) = -1/3$ $\psi_2(x,y) = 0$ $\psi_3(x,y) = 0$ $\psi_4(x,y) = -1$ $\psi_5(x,y) = +2$	$\varphi(x,y) = 1/6$ $\psi_1(x,y) = -1/3$ $\psi_2(x,y) = +1/2$ $\psi_3(x,y) = -1$ $\psi_4(x,y) = +1/2$ $\psi_5(x,y) = -1$

$f(x,y+\ell) = \langle f,\varphi\rangle$ $- \langle f,\psi_1\rangle$ $+ (\langle f,\psi_2\rangle$ $-\langle f,\psi_3\rangle/2)/2$ $+ (\langle f,\psi_4\rangle$ $-\langle f,\psi_5\rangle/2)/6$	$f(x+\ell,y+\ell) = \langle f,\varphi\rangle$ $- \langle f,\psi_1\rangle$ $+ 0$ $+ 0$ $- (\langle f,\psi_4\rangle$ $-\langle f,\psi_5\rangle/2)/3$	$f(x+2\ell,y+\ell) = \langle f,\varphi\rangle$ $- \langle f,\psi_1\rangle$ $- (\langle f,\psi_2\rangle$ $-\langle f,\psi_3\rangle/2)/2$ $+ (\langle f,\psi_4\rangle$ $-\langle f,\psi_5\rangle/2)/6$
$f(x,y) = \langle f,\varphi\rangle$ $+ \langle f,\psi_1\rangle$ $+ (\langle f,\psi_2\rangle$ $+\langle f,\psi_3\rangle/2)/2$ $+ (\langle f,\psi_4\rangle$ $+\langle f,\psi_5\rangle/2)/6$	$f(x+\ell,y) = \langle f,\varphi\rangle$ $+ \langle f,\psi_1\rangle$ $+ 0$ $+ 0$ $- (\langle f,\psi_4\rangle$ $+\langle f,\psi_5\rangle/2)/3$	$f(x+2\ell,y) = \langle f,\varphi\rangle$ $+ \langle f,\psi_1\rangle$ $- (\langle f,\psi_2\rangle$ $+\langle f,\psi_3\rangle/2)/2$ $+ (\langle f,\psi_4\rangle$ $+\langle f,\psi_5\rangle/2)/6$

FIGURE 3a: ***Constants in DWT and IDWT***

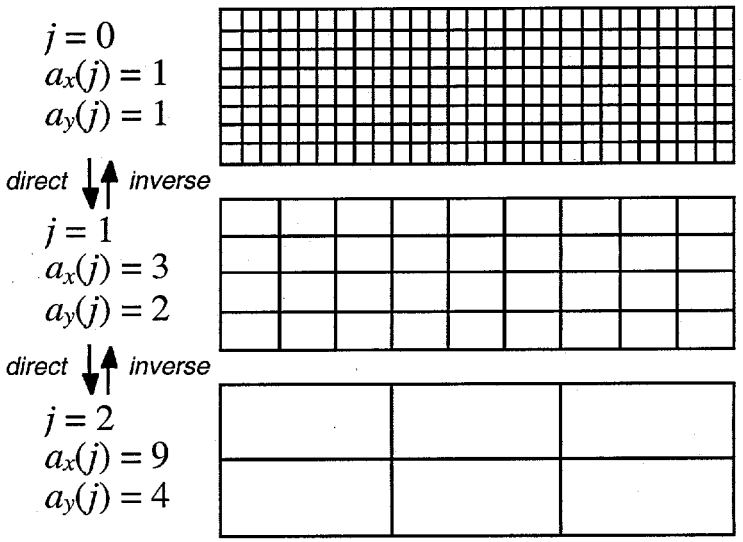

FIGURE 3b: ***Custom Anisotropic MRA***

Following the procedure outlined in §3, we can use the IDWT in Figs. 3a–b to generate anisotropic cascade models with radically different properties when integrated in the horizontal (#1) and vertical (#2) directions.

For instance, we can dial bounded cascade behavior in the horizontal and singular cascade behavior in the vertical, thus $\tau_1(q) \neq \tau_2(q)$. To achieve this, we take:

$T_{\varphi_3\psi_H}[\ln f](\boldsymbol{a}_j,\boldsymbol{b}_{ji}) = T_{\psi_H}[\cdot](a_{yj},\cdot)$ from Eq. (21a);

$T_{\psi_a\varphi_H}[\ln f](\boldsymbol{a}_j,\boldsymbol{b}_{ji}) = T_{\psi_a}[\cdot](a_{xj},\cdot)$ from Eq. (25a);

$T_{\psi_a\psi_H}[\ln f](\boldsymbol{a}_j,\boldsymbol{b}_{ji}) = 0$;

$T_{\psi_s\varphi_H}[\ln f](\boldsymbol{a}_j,\boldsymbol{b}_{ji}) = T_{\psi_s}[\cdot](a_{xj},\cdot)$ from Eq. (25b);

$T_{\psi_s\psi_H}[\ln f](\boldsymbol{a}_j,\boldsymbol{b}_{ji}) = 0$; and

$$T_{\varphi_3\varphi_H}[\ln f](\boldsymbol{a}_{j_{max}},\boldsymbol{0}) = \sum_j T_{\varphi_H}[\cdot](a_{xj},\cdot) + T_{\varphi_3}[\cdot](a_{yj},\cdot)$$

from (21b) and (25c) respectively. Figure 4 shows two specific 729×64 (n_c = 6) realizations of this model for $p_1 = 0.3$, $p_2 = 0.55$ and $H = 1/3$ horizontally, $p = 0.2$ and $H = 0$ in the vertical.

The choice of parameters and of marginal properties is not arbitrary: the Earth's cloudy atmosphere is strongly stratified and clouds tend to appear in well-defined layers —hence the singular model for the vertical unfolding— and in these layers long-range correlations are observed in the horizontal direction [8] —hence the bounded cascade (actually this was its very first application [17]). Recently developed radars that operate in at mm wave-lengths are able to probe vertical and horizontal cloud structure; we will apply the above MRA in analysis mode to such data in the near future.

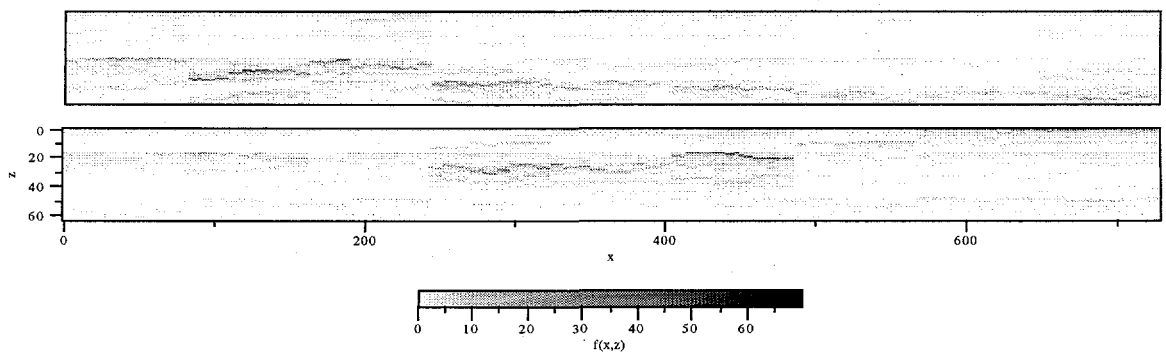

FIGURE 4: ***2 realizations of a highly anisotropic cascade generated by IDWT, with unit mean.***

5. SUMMARY

We surveyed, from an algorithmic stand-point, various ways of performing multifractal data analyses using wavelet transforms. The methods range from the sophisticated WTMM approach to the simplistic (yet overlooked) utilization of DWTs. The inevitable loss in robustness is offset by a significant gain in efficiency, thanks to Mallat's [1] algorithms.

Going from 1D to 2D, we show how a tensor product of dyadic and triadic DWTs can be used to simulate (here) and measure (in the near future) strong deviations from statistical isotropy, as are observed in many natural systems. Being highly stratified, the Earth's cloudy atmosphere is just one example.

REFERENCES

1. A. Arnéodo *et al.*, *Ondelettes, Multi-fractales et Turbulences – de l'ADN aux Croissances Cristalines* (Diderot, Paris, 1996); English version in preparation.
2. S. Mallat, *IEEE Trans. Pattern Anal. Mach. Intel.* **11**, 674 (1989)

3. A.S. Monin and A.M. Yaglom, *Statistical Fluid Mechanics*, Vol. 2 (MIT Press, Boston, 1975)
4. J.–F. Muzy, E. Bacry, and A. Arnéodo, *Phys. Rev. E* **47**, 875 (1993)
5. O. Rioul and M. Vetterli, *IEEE Signal Processing Magazine* **8**, 14 (1991)
6. J.–F. Muzy, E. Bacry, and A. Arnéodo, *Int. J. of Bifurcation and Chaos* **4**, 245 (1994); A. Arnéodo, E. Bacry, and J.–F. Muzy, *Physica A* **213**, 232 (1995)
7. T.C. Halsey *et al., Phys. Rev. A* **33**, 1141 (1986)
8. (a) A. Davis *et al., J. Atmos. Sci.* **53**, 1538–1558 (1996); (b) A. Marshak *et al., J. Atmos. Sci.* **54**, 1423 (1997)
9. R. Benzi *et al., Physica D* **65**, 352 (1993)
10. P. Flandrin, *IEEE Trans. Inform. Theory* **38**, 910 (1992)
11. A. Marshak *et al., Phys. Rev. E* **49**, 55 (1994)
12. B.B. Mandelbrot, *J. Fluid Mech.* **62**, 331 (1974)
13. C. Meneveau and K.R. Sreenivasan, *Phys. Rev. Lett.* **59**, 1424 (1987)
14. S. Mallat and W. L. Hwang, *IEEE Trans. Inform. Theory* **38**, 617 (1992); S. Mallat and S. Zhong, *IEEE Trans. Patt. Anal. Machine Intel.* **14**, 710 (1992)
15. G. Christakos, *Random Fields in Earth Sciences* (Academic, San Diego, 1992)
16. J. Arrault *et al., Phys. Rev. Lett.* **79**, 75 (1997)
17. R.F. Cahalan *et al., J. Atmos. Sci.* **51**, 2434 (1994)